Volume 19, Number 2, 2026. pp. 145-157

Jordan Journal of Physics

ARTICLE

Investigation of Magnetic and Thermoelectric Properties of New d^0 Full-Heusler Alloys

A. Yousfi[a], **A. Belli**[b], **H. Boulebda**[a] and **R. Temzini**[c]

[a] *Laboratoire d'Etudes et Développement des Matériaux Semiconducteurs et Diélectriques, Faculté de Technologie, Université Amar Telidji, Laghouat, (03000), Algeria.*

[b] *Laboratoire des Matériaux Magnétiques, Faculté des Sciences Exactes, Université Djillali Liabès de Sidi Bel-Abbès, Sidi Bel-Abbès (22000), Algeria.*

[c] *Laboratory of Materials, Applications and Valorization of Renewable Energy (LMAVER), University Amar Telidji, Laghouat, 03000, Algeria.*

DOI: **https://doi.org/10.47011/19.2.4**

Received on: 09/10/2024; *Accepted on: 29/04/2025*

Abstract: The structural, optoelectronic, magnetic, and thermoelectric properties of $CsYO_2$ (Y = Li, Na and K) full-Heusler alloys have been investigated using density functional theory (DFT). All three alloys were found to be stable in the ferromagnetic state with the $AlCu_2Mn$-type structure. The band structure plots showed a gap in the spin-up channel, whereas the spin-down channel exhibited an overlap between the Fermi level and the valence band, indicating half-metallic behavior. The PDOS revealed that oxygen is the primary contributor to the total magnetic moment, which was found to have an integer value. The compounds obey the Slater-Pauling rule, expressed as $M_t = Z - 12$, where Z represents the number of valence electrons (Z = 14), resulting in a total magnetic moment of 2.0 μB for $CsLiO_2$, $CsNaO_2$, and $CsKO_2$ compounds. The optical and thermoelectric properties were also investigated and analyzed.

Keywords: Heusler alloys, DFT calculations, Electronic properties, Magnetic properties.

1. Introduction

The field of electronics has experienced significant advances over the past few decades, particularly in data storage and transfer technologies. In this field, spintronics has emerged as an efficient technology. Due to their special properties, half-metallic materials are heavily exploited in spintronics (spin injection, giant magnetoresistance GMR, magnetic tunnel junction TMR, etc.) [1-4]. With 100% of spin polarizability, half-metallic ferromagnets must exhibit a gap in one spin orientation and metallic conduction in the other [4, 5]. De Groot et al. [6] reported the first study on the half-metallic ferromagnet NiMnSb. Numerous half-metal materials with Heusler structures have been explored through both theoretical and experimental approaches since the discovery of Heusler alloys by Friedrich Heusler [7, 8]. Heusler alloys are among the favorable intermetallic alloys [9]. The high Curie temperature (Tc) and 100% spin polarizability of Heusler alloys, whether they are full-Heusler X_2YZ or half-Heusler XYZ (where Z is typically a semiconductor or a sp element) make them strong candidates for spintronic applications.

Thus far, the majority of research on half-metallic Heusler alloys has focused on 3d transition-metal elements (for example, V, Cr, Mn, etc.) [10-21], with comparatively fewer studies examining 4d transition metal elements (like Zr-base alloys, Etc...). [22], and even fewer papers involving 5d transition-metal elements (such as V_2ReZ) were published [23]. Recent research has focused on developing new half-metals, or so-called sp or d^0 half-metallic materials, such as $CsBaX_2$ (X = C, N, and O) [5],

Corresponding Author: A. Belli **Email**: ayoubbelli03@gmail.com

$RbSrX_2$ (X = C, N, and O), $KCaX_2$ (X = C, N, and O), and RbSrZ (Z = C, Si, and Ge) [24, 25]. These compounds do not contain transition metal elements.

In this context, we decided to examine the full-Heusler alloys $CsLiO_2$, $CsNaO_2$ and $CsKO_2$, excluding the use of transition metal elements (d^0 half metallic alloys), and compare the results with other theoretical studies. We hope this work motivates other researchers in the future to continue research in this field.

2. Calculation Method

The investigation of $CsYO_2$ (Y = Li, Na et K) alloys was performed using the full-potential linearized augmented plane wave (FP-LAPW) method implemented in the WIEN2k code [26]. The exchange–correlation potential was treated using the generalized gradient approximation (GGA-PBE) [27]. The parameter $R_{mt}K_{max}$ was set to 8.5, where Rmt indicates the smallest radius of the muffin-tin spheres, and Kmax refers to the cutoff for the wave function basis set. The Rmt values were automatically determined. The wave-function expansion inside the spheres was carried out up to lmax = 12, while the charge density was expanded in Fourier series up to Gmax = 14 (a.u). The selected cut-off energy was − 6 (*Ry*). The k-points used in the irreducible Brillouin zone (BZ) were 3000. For the dielectric-function calculations, a dense k-point mesh of 10,000 k-points in the Brillouin zone (BZ) was used to achieve satisfactory convergence and improved precision at high-symmetry points.

3. Results and Discussion

3.1. Structural Stability

It is widely recognized that full-Heusler compounds possess a 2:1:1 stoichiometric ratio and crystallize in two possible structures, AlCu2Mn-type (L21) structure with space group $Fm\bar{3}m$ (No. 225), and Cu2HgTi-type structure with space group $F\bar{4}3m$ (No. 216). The atomic occupancies for the $AlCu_2Mn$-type are as follows: 4a (0,0,0), 4b (0.5,0.5,0.5), 8c (0.25,0.25,0.25), for Cs, Y, and O, respectively, while for the Cu2HgTi-type structure, Cs occupies the 4d (0.75,0.75,0.75), Y is 4b (0.5,0.5,0.5), O is 4a (0,0,0), and 4c (0.25,0.25,0.25). Figure 1 illustrates the atomic occupancies of CsNaO2 in both structural configurations.

FIG. 1. Crystal structures of CsNaO2 in the AlCu2Mn-type and Cu2HgTi-type Heusler phases.

The total energies as a function of unit-cell volume for the AlCu2Mn-type and Cu2HgTi-type structures in both ferromagnetic (FM) and paramagnetic (PM) states were calculated and fitted to the Birch-Murnaghan equation of state [28] to determine the ground-state structure and evaluate the structural parameters of $CsLiO_2$, $CsNaO_2$, and $CsKO_2$ compounds. The calculated total-energy curves are shown in Fig. 2.

$$E(V) = E_0 + \frac{9V_0B_0}{16}\left\{\left[\left(\frac{V_0}{V}\right)^{2/3} - 1\right]^3 B_0' + \left[\left(\left(\frac{V_0}{V}\right)^{2/3} - 1\right)\right]^2 \left[6 - 4\left(\left(\frac{V_0}{V}\right)^{2/3}\right)\right]\right\} \quad (1)$$

In Eq. (1), V_0, E_0 and B_0 represent the equilibrium unit-cell volume, total energy, and bulk modulus, respectively. The term $E(V)$ denoted the total energy per unit cell as a function of volume, while B_0 denotes the pressure derivative of the bulk modulus.

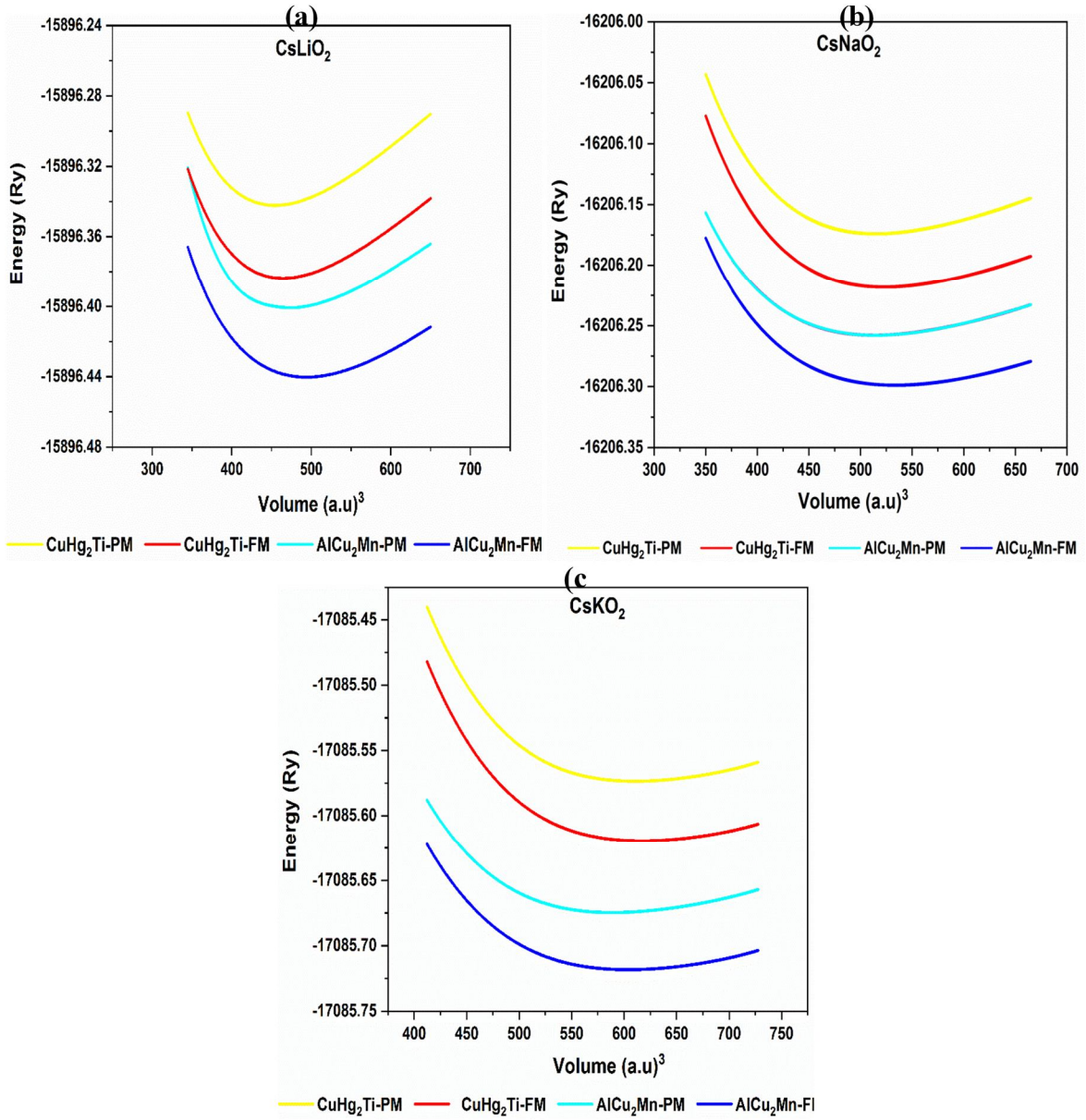

FIG. 2. Calculated total-energy curves versus unit-cell volume for CsLiO2 (a), CsNaO2 (b), and CsKO2 (c) Heusler alloys.

The alloy energies were calculated in the ferromagnetic and paramagnetic states within two structural types (AlCu2Mn-type and Cu2HgTi-type). It was found from Fig. 2 that the ferromagnetic state is more stable than the paramagnetic state for both structures. Moreover, the alloys exhibited greater stability in the ferromagnetic state within the Cu_2MnAl-type structure compared to the same state within the Hg_2CuTi-type. Therefore, AlCu2Mn-type phase was considered the stable ground-state structure for the subsequent property calculations of all compounds.

Table 1 summarizes the structural parameters of the stable ground-state configurations of $CsLiO_2$, $CsNaO_2$, and $CsKO_2$ alloys, obtained by minimizing the total energy as a function of volume, using the Murnaghan equation of state. Due to the absence of available theoretical and experimental data, comparisons with related theoretical studies were used to validate the obtained results.

TABLE 1. Calculated structural parameters, including the equilibrium lattice constant a (Å), bulk modulus B (*GPa*), pressure derivative of the bulk modulus B′, cohesive energy E_c (*Ry*), and formation energy E_f (*Ry*).

Compound	Structure	a	B	B'	E_c	E_f
$CsLiO_2$	$AlCu_2Mn$	6.62	25.78	4.01	-3.45	-1.67
$CsNaO_2$	$AlCu_2Mn$	6.8	25.43	4.59	-1.01	-0.51
$CsKO_2$	$AlCu_2Mn$	7.1	22.34	4.68	-1.02	-0.55
$CsCaO_2$[40]	$AlCu_2Mn$	6.6	--	--	--	--
$CsBaO_2$[40]	$AlCu_2Mn$	7.0	--	--	--	--

The cohesive energy E_c evaluates the strength of the forces binding atoms together in the solid phase.

$$E_c^{CsYO_2} = E_{tot}^{CsYO_2} - (E_{Cs} + E_Y + 2E_O) \quad (2)$$

$E_c^{CsYO_2}$ represents the equilibrium total energy of the $CsYO_2$ compounds, and E_{Cs}, E_Y, E_O denote the total energies of the isolated atoms.

The calculated E_c values are -3.45, -1.01, and -1.02 (*Ry*) for $CsLiO_2$, $CsNaO_2$, and $CsKO_2$ compounds, respectively, confirming the structural stability of the alloys.

The formation energy E_f is defined as the difference between the total energy of the compound and the total energies of its constituent elements in their bulk phases.

$$E_f^{CsYO_2} = E_{tot}^{CsYO_2} - \left(E_{Cs}^{bulk} + E_Y^{bulk} + 2E_O^{bulk}\right) \quad (3)$$

where $E_f^{CsYO_2}$ is the equilibrium total energy of $CsYO_2$ compounds and $E_{Cs}^{bulk}, E_Y^{bulk}, E_O^{bulk}$ represent the total energies of the constituent atoms in their bulk phases.

The calculated E_f values are -1.67, -0.51, and -0.55 (*Ry*) for $CsLiO_2$, $CsNaO_2$, and $CsKO_2$ compounds, respectively, indicating that the studied alloys are thermodynamically stable against decomposition. The negative values of the cohesive energy (E_c) and formation energy (E_f), summarized in Table 1, suggest that $CsLiO_2$, $CsNaO_2$, and $CsKO_2$ compounds may be synthesized experimentally.

3.2. Electronic and Optical Properties

In order to investigate the electronic behavior, half-metallicity, and spin polarization of $CsLiO_2$, $CsNaO_2$, and $CsKO_2$ compounds, the band structure (BS) and density of states (DOS) were calculated. The band structure of all compounds for both spin-up and spin-down channels, calculated at the equilibrium lattice constant and along the high-symmetry points of the first Brillouin zone, are shown in Fig. 3.

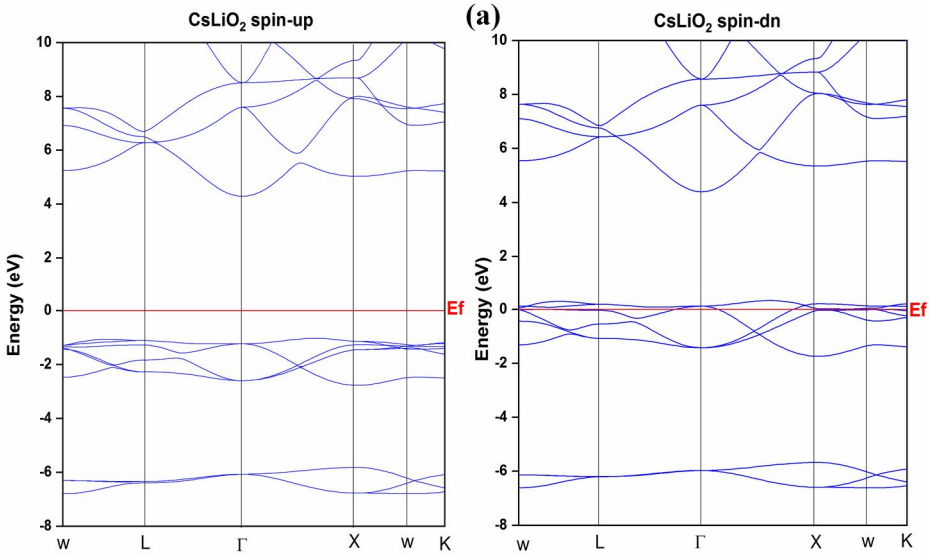

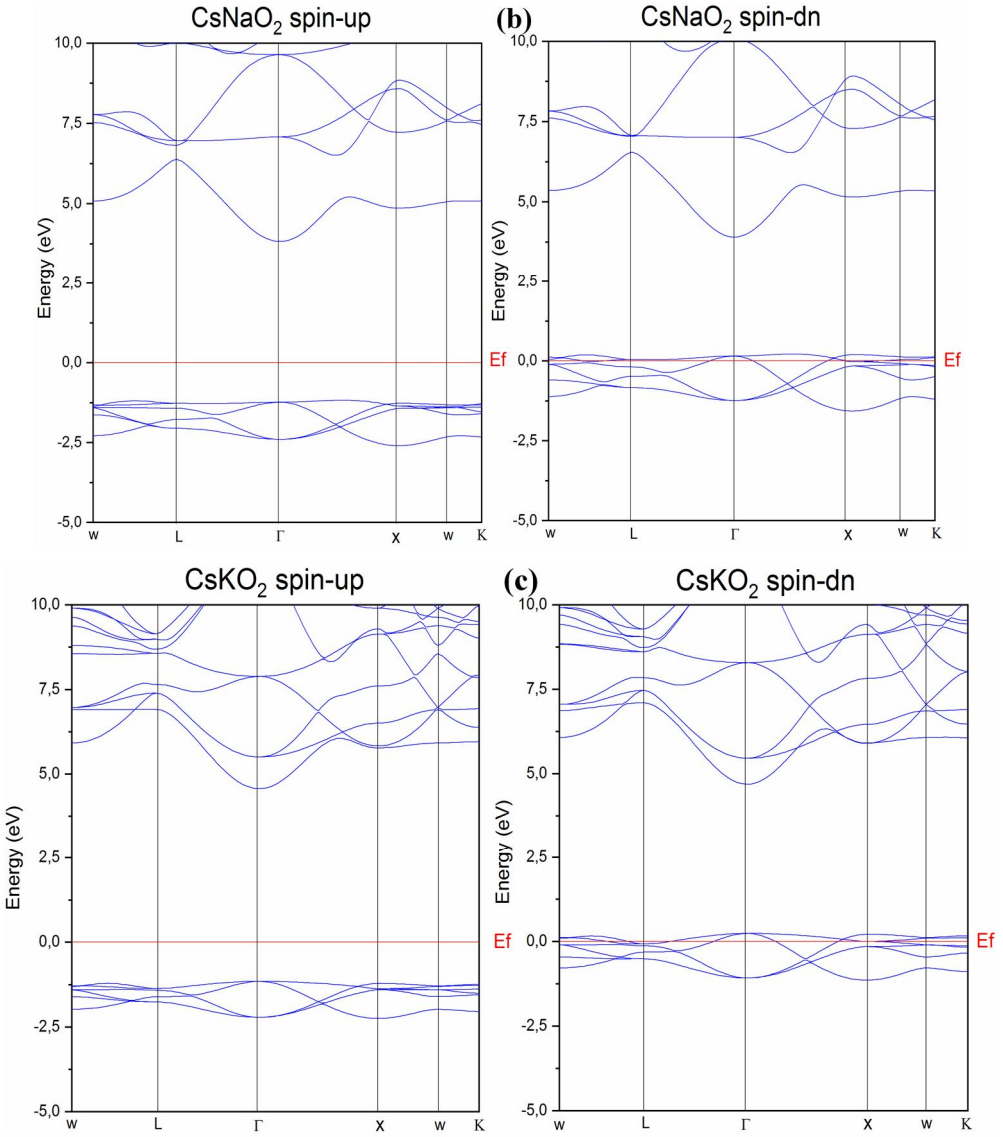

FIG. 3. The spin-up and spin-down band structures of $CsLiO_2$ (a), $CsNaO_2$ (b) and $CsKO_2$ (c) Heusler alloys.

It can be observed from the band structures that a gap exists around the Fermi level in the majority-spin channel, while an intersection is observed between the valence band and the Fermi level. The combined behavior of the two spin channels together confirms the presence of half-metallic behavior in our alloys. Furthermore, the spin polarization of our compounds reaches 100% at the Fermi level according to the spin polarizability expression $p = \frac{n\uparrow(E_f) - n\downarrow(E_f)}{n\uparrow(E_f) + n\downarrow(E_f)} \times 100$ where $n\uparrow(E_f)$ and $n\downarrow(E_f)$ are the spin-dependent densities of states around the fermi level [29], and this is also strong evidence for the half-metallic character. It can also be observed from the band structure of $CsLiO_2$ and $CsNaO_2$ indirect band gaps equal to 5.07 eV and 4.9 eV, respectively, whereas for $CsKO_2$ the band gap is direct and has a value of 5.7 eV. In addition, the band-gap energy is defined as the difference between the minimum energy level of the conduction band and the maximum energy level of the valence band. Moreover, the half metallic gap E_{HMg} is the difference between the highest energy of the valence band in the semiconducting channel and the fermi level. The half metallic gaps are 1.08, 1.17 and 1.15, for $CsLiO_2$, $CsNaO_2$ and $CsKO_2$ respectively. The Ebg and E_{HMg} values are listed in Table 2. The data of our half-metallic compounds are considerably larger than those of half-metallic Heusler alloys composed of transition metals, which means a stronger resistance to the destruction of half-metallicity destruction under pressure or temperature variations.

TABLE 2. Calculated total magnetic moments (M_{tot}), and atomic magnetic moments (M_a) per formula unit, size of the band gap (Ebg), and the half-metallic gap (E_{HM}).

Compound	Ebg (eV)	E_{HM} (eV)	M_{Cs} (μB)	M_Y (μB)	M_O (μB)	M_{tot} (μB)
$CsLiO_2$	5.07	1.08	0.084	-0.005	0.909	2
$CsNaO_2$	4.9	1.17	0.052	-0.011	0.988	2
$CsKO_2$	5.7	1.15	0.024	-0.004	0.995	2
N_2BaCs[41]	4.6	2.33	--	--	--	--
N_2BaRb[41]	5.44	2.39	--	--	--	--

To provide a deeper explanation of the electronic properties, we present the total density of states (TDOS) and partial density of states (PDOS) of all compounds in Fig. 4.

According to Fig. 4, the TDOS of the compounds exhibits a clear gap in the spin-up channel with 100% spin polarization at the Fermi level, which confirms the half-metallic behavior comportment of $CsLiO_2$, $CsNaO_2$ and $CsKO_2$ compounds. The partial densities of states around the Fermi level of all our alloys are mainly dominated by O-*p* states in both directions. In the energy range between -8 and -6 eV, there is an evident contribution due to Cs-*p* states for all compounds. The energy interval from 5 to 10 eV shows almost identical DOS for both spin directions for $CsLiO_2$, $CsNaO_2$ and $CsKO_2$ compounds originating from the Cs, Li, Na, K, and O atoms.

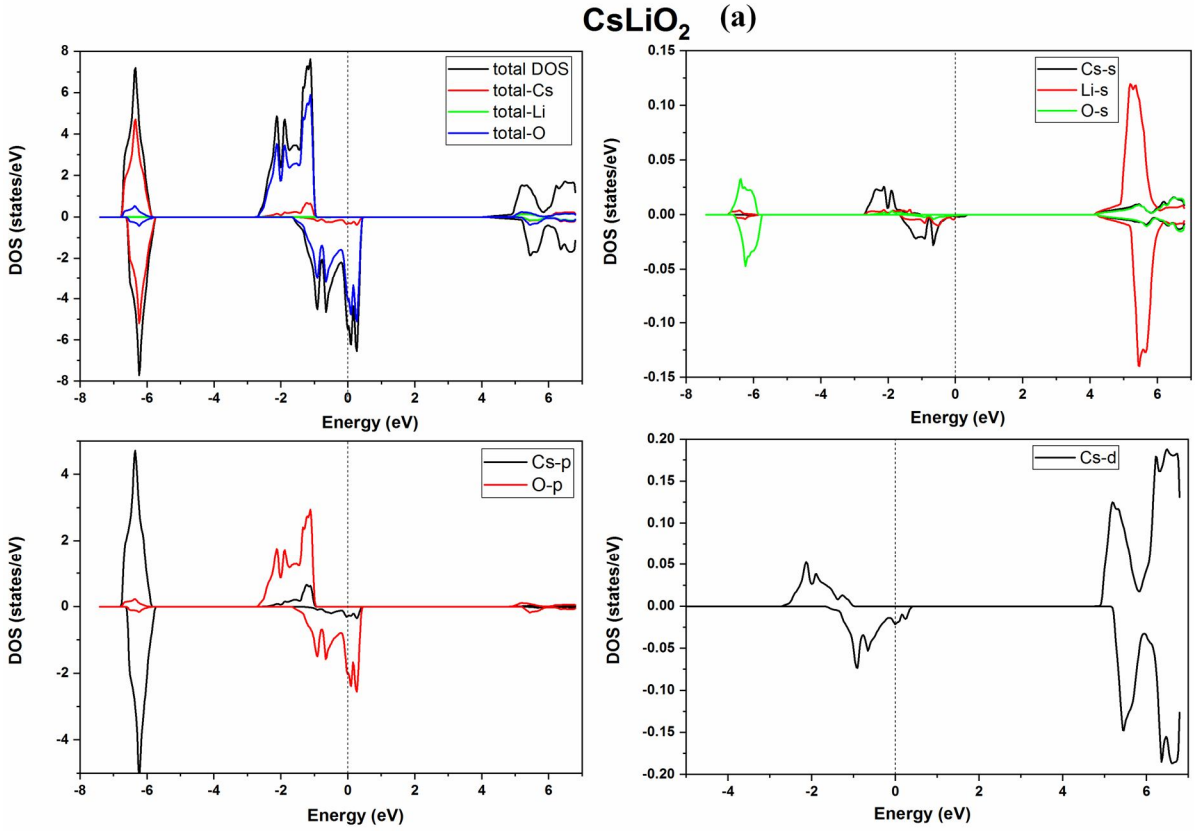

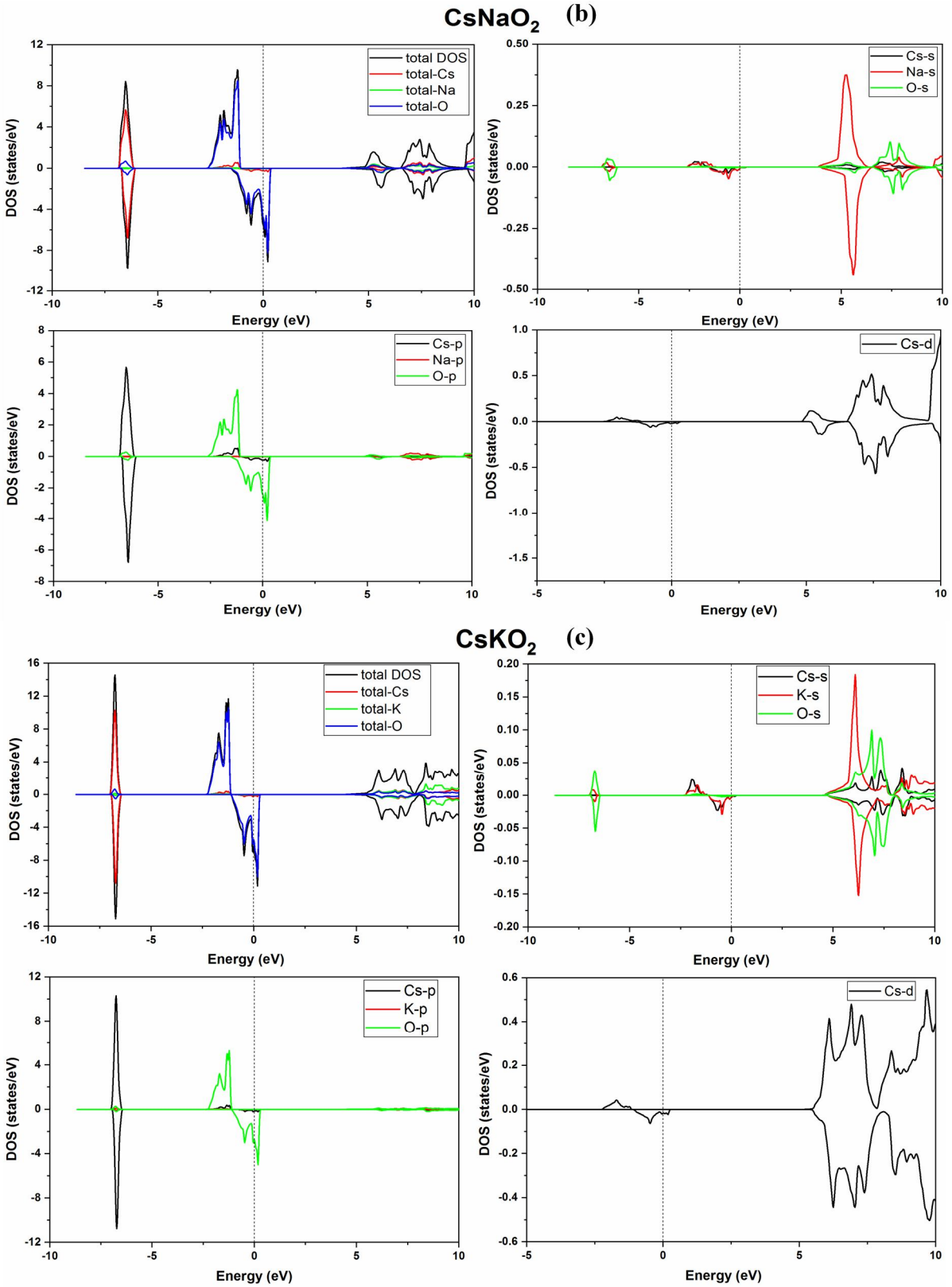

FIG. 4. The total and partial densities of states of $CsLiO_2$ (a), $CsNaO_2$ (b) and $CsKO_2$ (c) Heusler compounds.

The complex dielectric functions of the compounds under study and their corresponding derivatives for both spin channels are also computed to provide further information on the electronic structure. For the optical spectra, 10000 k-points were used to compute the dielectric functions in the Brillouin zone.

The calculated imaginary (ε_2) and real (ε_1) parts of the optical dielectric function imaginary

are displayed in Fig. 5 as functions of photon energy values, which range from 0.0 to 14.0 eV. The imaginary part demonstrates that, in the spin-up state, $CsLiO_2$, $CsNaO_2$ and $CsKO_2$ compounds have an optical gap. These findings support what we had previously discovered about the half-metallic nature in the spin-down channel and semiconducting character in the spin-up channel. The spin-down state also exhibits a significant increase at low energies, due to indirect intraband excitations. This result is consistent with the HMF gap in the spin-up band structure and agrees with our earlier findings.

3.3. Magnetic Properties

The effect of pressure on magnetic moments is a well-studied phenomenon in materials science, particularly for ferromagnetic and antiferromagnetic materials. As pressure is applied to an alloy (often by changing the lattice parameter), the magnetic properties of the material can be significantly influenced. This is because pressure changes the interatomic distances, which can affect the electronic structure and interactions between magnetic moments. Therefore, we have estimated the total and atomic magnetic moments as function of the lattice parameter. According to Table 2 the principal contributor to the M_{tot} for all alloys is the O atoms, while the other atoms may be considered negligible contributors due to the negative values that approach zero, indicating that our compounds are ferromagnetic half metals. It was also found that the total magnetic moments are integer values and equal to 2 (μB) for all compounds, satisfying the Slater Pauling rule [30] but different from the conventional form; $M_{tot} = Z - 24$ (where M_t is the total magnetic moment per unit cell and Z is the number of valence electrons). In our case the number of valence electrons for all compounds is Z = 14, with electronic configurations as follows: Cs: $6s^1$, Li:$2s^2$, Na: $3s^{1,}$ K: $4s^{1,}$ O: $2s^2$ $2p^4$. Thus, the Slater-Pauling rule satisfied by $CsLiO_2$, $CsNaO_2$ and $CsKO_2$ can be expressed as: $M_t = Z - 12$.

More specifically, four valence electrons occupy the O-2*s* states at the lowest energy levels, resulting in six of the remaining ten valence electrons occupying the majority spin *p* states of O, which results in six fully occupied majority-spin bands. Furthermore, the remaining four valence electrons partially occupy the six lowest minority-spin bands, leaving two holes, which are responsible for the total magnetic moment of 2μB in the three compounds.

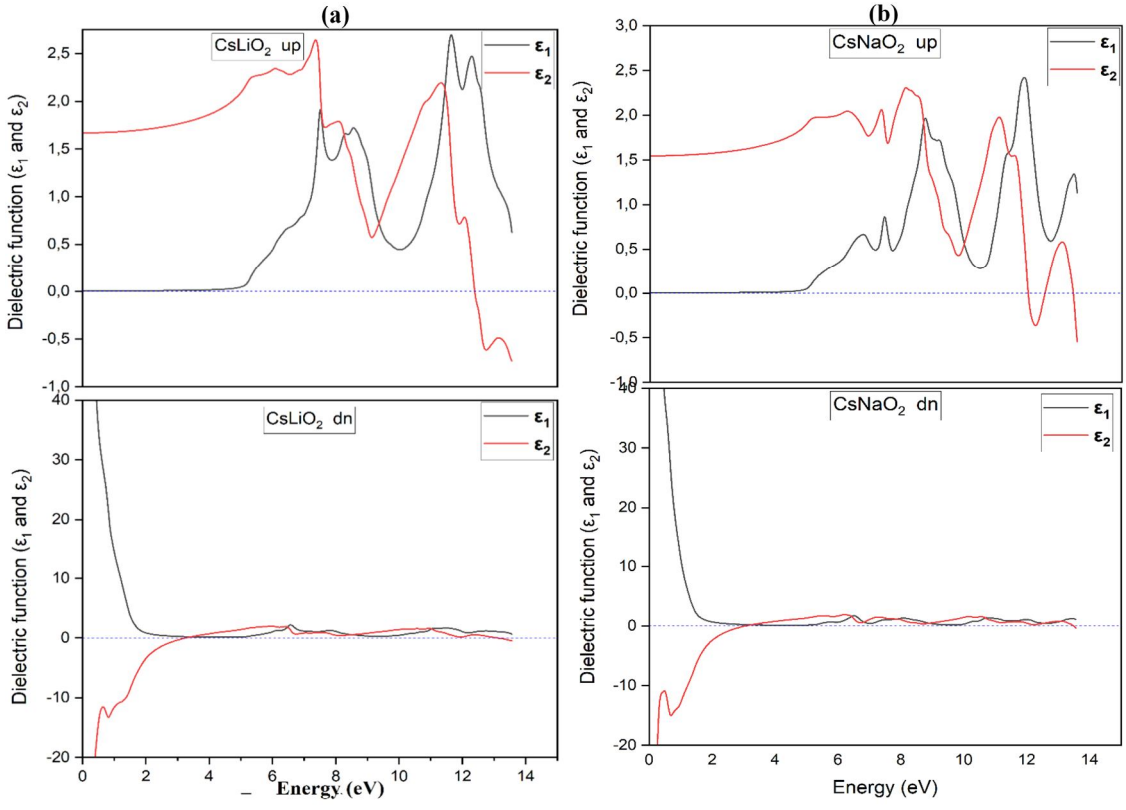

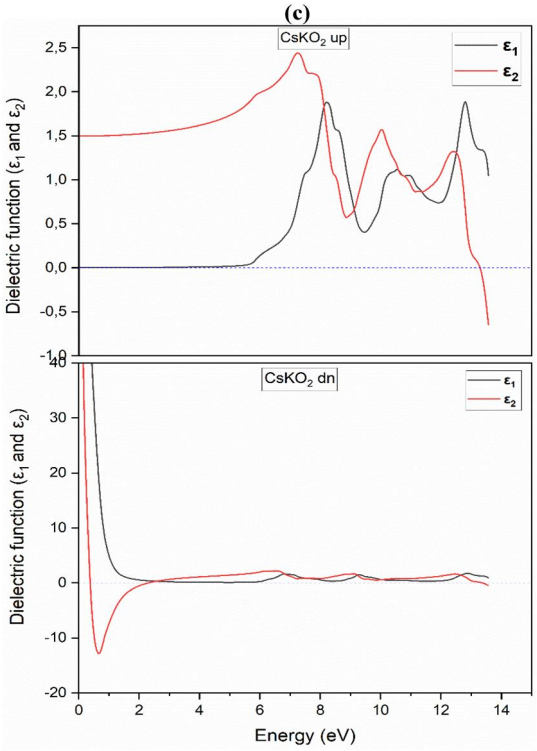

FIG. 5. The real and the imaginary dielectric function parts for $CsNaO_2$, $CsKO_2$, and $CsLiO_2$ Heusler alloys.

Fig. 6 illustrates the contributions of the atoms in the three alloys to the atomic and total magnetic moment (M_{tot}) originates from the atomic magnetic moments of the oxygen atoms, as mentioned previously, reaching 1μB at the equilibrium lattice parameter.

Regarding the other elements (Li, Na, K), slight increases and decreases can be observed; however, their values remain very small, allowing them to be considered negligible contributors.

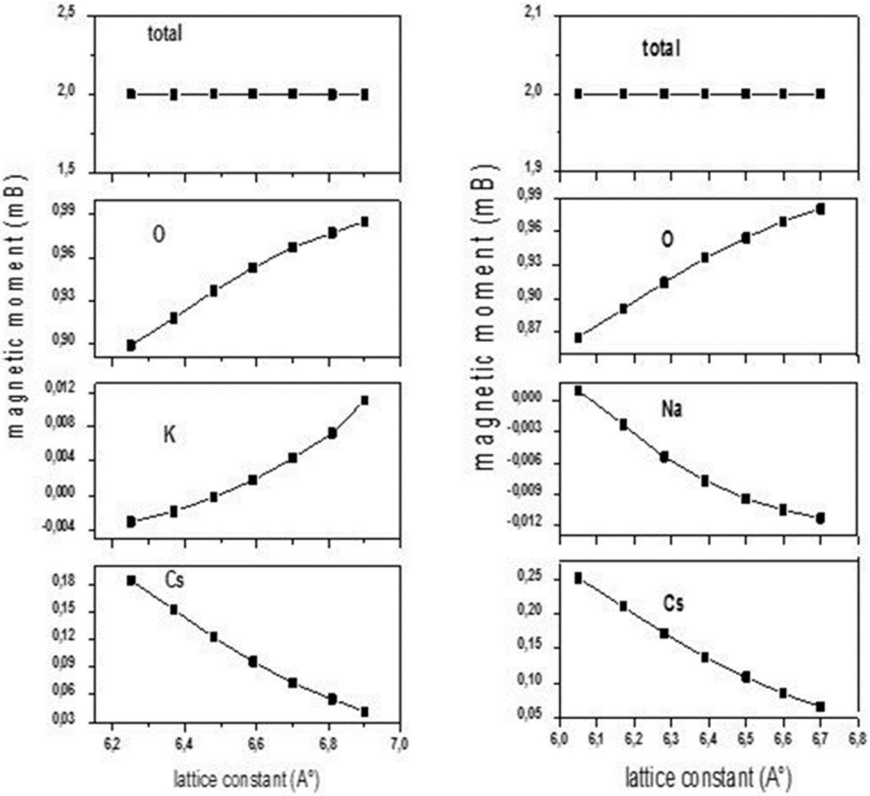

FIG. 6. The total and atomic magnetic moments as functions of the lattice parameter.

3.4. Thermoelectric Properties

To further highlight the potential of our half-metallic compounds, we employed the BoltzTraP package integrated into the WIEN2k code to calculate several thermoelectric parameters. The BoltzTraP package [31] is widely recognized for its implementation of the Boltzmann transport equation across multiple fields, including superconductors [32], intermetallic phases [33], and particularly thermoelectric research [34-37].

The transport properties of the $CsYO_2$ compounds (Y = Na, Li, K) at different temperatures, as functions of chemical potential, are presented in Fig. 7. Figure 7 shows that the electrical conductivity approaches zero around the Fermi level, which is characteristic behavior of semiconductors. Due to intrinsic excitations in half-metals, the electrical conductivity increases significantly with increasing temperature. For positive chemical potentials, the electrical conductivity per unit time (s/t) is nearly identical to that obtained for negative chemical potentials, suggesting that the conductivities of n-type and p-type materials are nearly equivalent.

As shown in Fig. 7, the power factor (PF) increases with increasing temperature, and the highest PF values for all studied compounds occur in the p-type region. Furthermore, the maximum PF at positive chemical potentials is greater than that at negative chemical potentials, indicating that the p-type compounds exhibit better thermoelectric performance than the n-type compounds in $CsYO_2$.

The dimensionless figure of merit (ZT) is an important parameter for evaluating the efficiency of thermoelectric materials. The thermoelectric performance can be estimated using the following expression:

$$Zt = \sigma S^2 T/\kappa.$$

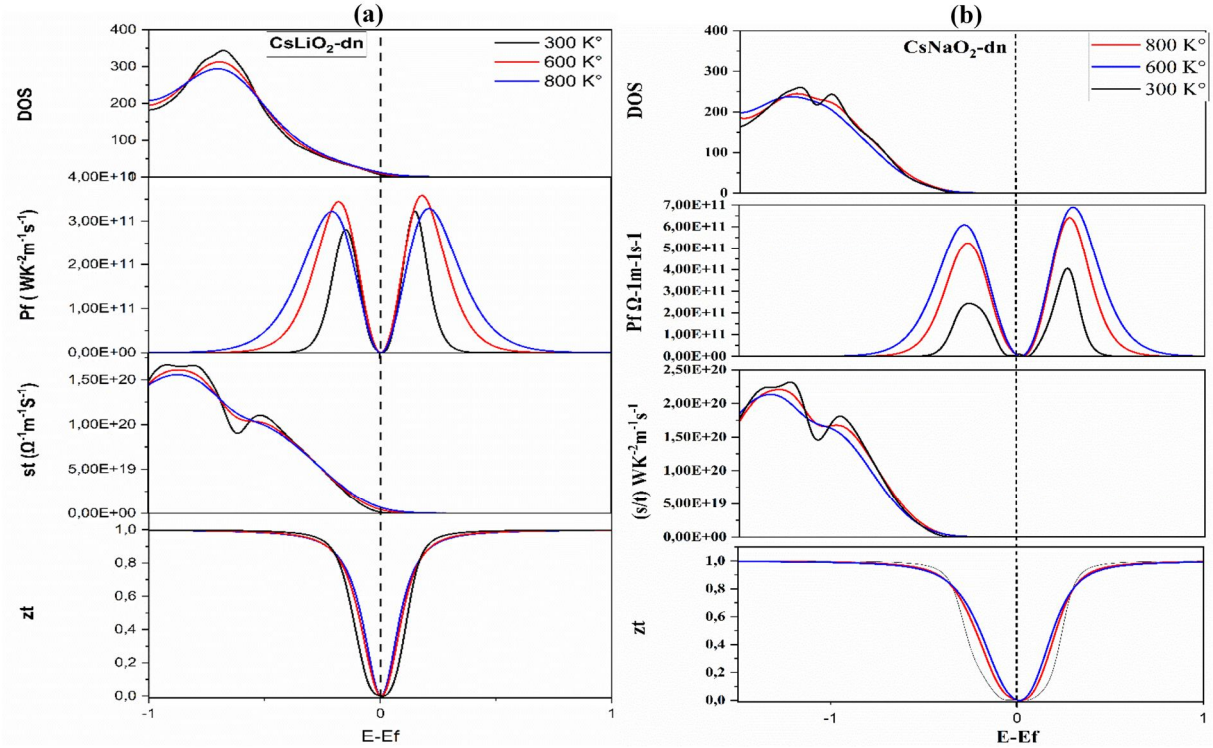

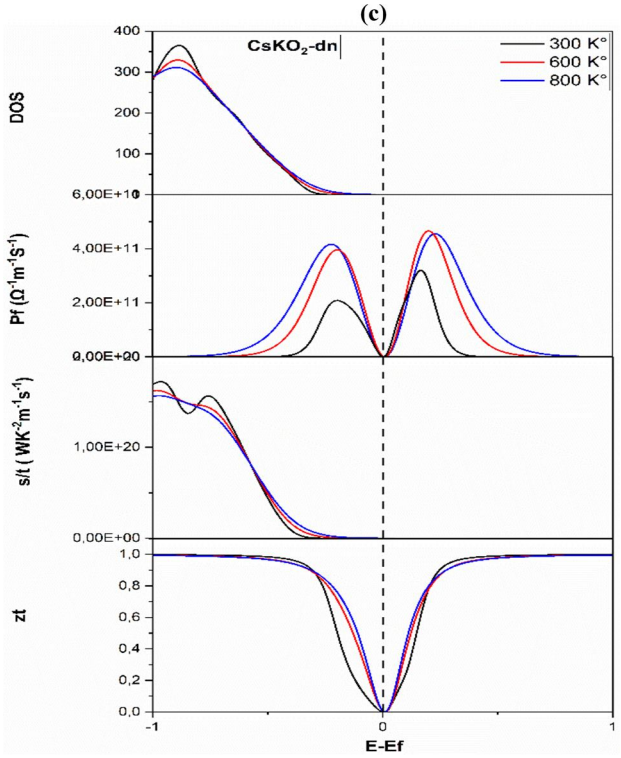

FIG. 7. The thermoelectric parameters; DOS, Seebeck coefficient, electrical conductivity, and figure of merit.

It is well established that materials with ZT ≈ 1 are considered promising candidates for thermoelectric applications [38, 39]. Figure 7 shows the variation of ZT as a function of the chemical potential for $CsYO_2$, exhibiting approximately similar behavior for the three studied compounds. For all compounds, ZT is very close to unity at room temperature. However, it decreases sharply and reaches a minimum value of zero within the chemical-potential range of -0.25, +0.25 eV for $CsNaO_2$, $CsKO_2$, and $CsLiO_2$.

The DOS curves indicate that the half-metallic character is preserved up to 800 K°, providing additional evidence supporting the classification of these compounds as half-metals.

4. Conclusion

First-principles calculations were performed to design new d^0 full-Heusler compounds, $CsYO_2$ (Y = Li, Na, and K), using the full-potential linearized augmented plane wave (FPLAPW) method based on density functional theory, as implemented in the WIEN2k code. The study reveals that $CsLiO_2$, $CsNaO_2$, and $CsKO_2$ compounds are energetically favorable in the ferromagnetic state within the $AlCu_2Mn$-structure. The band structures, the density-of-states calculations, showing 100% spin polarization around the Fermi level, clearly demonstrate the half-metallic character of all compounds. This behavior is further confirmed by the integer magnetic moments equal to 2μB, as well as by the optical gap observed in the imaginary part (ε_2) of the dielectric function.

The main contribution to the total magnetic moment originates from the oxygen atoms. Since the negative atomic magnetic moments of Li, Na, and K are very small compared with the positive magnetic moment of oxygen, the compounds can be classified as half-metallic ferromagnets.

Furthermore, the thermoelectric figure of merit (ZT) approaches unity, indicating remarkable thermoelectric efficiency.

Acknowledgements

This work was funded by DGRSDT (The General Directorate for Scientific Research and Technological Development).

Declaration of conflict interests

The authors declare that they have no known competing financial interests or personal relationships or conflicts that could have appeared to influence the work reported in this paper.

References

[1] Xie, W.-H., Xu, Y.-Q., Liu, B.-G., and Pettifor, D., Physical Review Letters, 91 (2003) 037204.

[2] Fan, L., Chen, F., and Chen, Z.-Q., Journal of Magnetism and Magnetic Materials, 478 (2019) 264.

[3] Rasul, M.N., Javed, A., Khan, M.A., and Hussain, A., Journal of Magnetism and Magnetic Materials, 476 (2019) 398.

[4] Ayhan, S. and Kavak Balcı, G., Materials Research Express, 6 (2019) 0865.

[5] Erfan, Z. and Ahmadian, F., Journal of Superconductivity and Novel Magnetism, 28 (2015) 3301.

[6] De Groot, R., Mueller, F., van Engen, P.V., and Buschow, K., Physical Review Letters, 50 (1983) 2024.

[7] Heusler, F., Deutsche Physikalische Gesellschaft (DPG), 5 (1903) 219.

[8] Ayhan, S. and Balcı, G.K., AIP Conference Proceedings, AIP Publishing, (2018).

[9] Ouahdani, A., Takassa, R., Elfatouaki, F., Farkad, O., Hassine, S., El Mouncharih, A., Choukri, O., Ibnouelghazi, E., Abouelaoualim, D., Jordan Journal of Physics, 17 (2024) 331.

[10] Rostami, M., Moradi, M., Javdani, Z., and Salehi, H., Materials Science in Semiconductor Processing, 38 (2015) 218.

[11] Chen, X.-Q., Podloucky, R., and Rogl, P., Journal of Applied Physics, 100 (2006) 113901.

[12] Özdog, K., Galanakis, I., Şaşıog, E., and Aktaş, B., Solid State Communications, 142 (2007) 492.

[13] Sharma, V., Solanki, A., and Kashyap, A., Journal of Magnetism and Magnetic Materials, 322 (2010) 2922.

[14] Liu, G., Dai, X., Liu, H., Chen, J., Li, Y., Xiao, G., and Wu, G., Physical Review B, 77 (2008) 014424.

[15] Kervan, N. and Kervan, S., Intermetallics, 24 (2012) 56.

[16] Kervan, N. and Kervan, S., Intermetallics, 37 (2013) 88.

[17] Galanakis, I., Özdoğan, K., Şaşıoğlu, E., and Aktaş, B., Physical Review B, 75 (2007) 172405.

[18] Li, J., Li, Y., Zhou, G., Sun, Y., and Sun, C.Q., Applied Physics Letters, 94 (2009) 131902.

[19] Xing, N., Gong, Y., Zhang, W., Dong, J., and Li, H., Computational Materials Science, 45 (2009) 489.

[20] Wei, X.-P., Deng, J.-B., Mao, G.-Y., Chu, S.-B., and Hu, X.-R., Intermetallics, 29 (2012) 86.

[21] Belli, A., Cheref, O., Rached, H., Caid, M., Guermit, Y., Rached, D., Rabah, M., Abidri, B., and Khenata, R., Pramana, 95 (2021) 61.

[22] Xie, H.-H., Gao, Q., Li, L., Lei, G., Mao, G.-Y., Hu, X.-R., and Deng, J.-B., Computational Materials Science, 103 (2015) 52.

[23] Jia, H., Dai, X., Zhang, X., Wang, L., Chen, L., Wang, F., Jia, M., and Liu, G., Journal of Magnetism and Magnetic Materials, 343 (2013) 268.

[24] Rozale, H., Lakdja, A., Amar, A., Chahed, A., and Benhelal, O., Computational Materials Science, 69 (2013) 229.

[25] Bagverdi, F. and Ahmadian, F., Journal of Superconductivity and Novel Magnetism, 28 (2015) 2773.

[26] Schwarz, K. and Blaha, P., Computational Materials Science, 28 (2003) 259.

[27] Perdew, J.P., Burke, K., and Ernzerhof, M., Physical Review Letters, 77 (1996) 3865.

[28] Murnaghan, F.D., Proceedings of the National Academy of Sciences, 30 (1944) 244.

[29] Soulen Jr, R., Byers, J., Osofsky, M., Nadgorny, B., Ambrose, T., Cheng, S., Broussard, P.R., Tanaka, C., Nowak, J., and Moodera, J., Science, 282 (1998) 85.

[30] Galanakis, I., Dederichs, P., Papanikolaou, N., Physical Review B, 66 (2002) 174429.

[31] Madsen, G.K. and Singh, D.J., Computer Physics Communications, 175 (2006) 67.

[32] Madsen, G. and Singh, D.J., Computer Physics Communications, 175 (2006) 67.

[33] Dolinšek, J., Komelj, M., Jeglič, P., Vrtnik, S., Stanić, D., Popčević, P., Ivkov, J., Smontara, A., Jagličić, Z., and Gille, P., Physical Review B—Condensed Matter and Materials Physics, 79 (2009) 184201.

[34] Luo, D.B., Wang, Y.X., Yan, Y.L., Yang, G., Yang, J.M., Journal of Materials Chemistry A, 2 (2014) 15159.

[35] May, A.F., Singh, D.J., and Snyder, G.J., Physical Review B—Condensed Matter and Materials Physics, 79 (2009) 153101.

[36] Ouardi, S., Fecher, G.H., Balke, B., Kozina, X., Stryganyuk, G., Felser, C., Lowitzer, S., Ködderitzsch, D., Ebert, H., and Ikenaga, E., Physical Review B—Condensed Matter and Materials Physics, 82 (2010) 085108.

[37] Parker, D., Chen, X., and Singh, D.J., Physical Review Letters, 110 (2013) 146601.

[38] Bainsla, L., Yilgin, R., Okabayashi, J., Ono, A., Suzuki, K., and Mizukami, S., Physical Review B, 96 (2017) 094404.

[39] Dai, X., Liu, G., Fecher, G.H., Felser, C., Li, Y., and Liu, H., Journal of Applied Physics, 105 (2009) 07E901.

[40] Gao, Y. and Wang, X., Journal of the Korean Physical Society, 66 (2015) 1160.

[41] Benatmane, S. and Bouhafs, B., Computational Condensed Matter, 19 (2019) e00371.